ELSEVIER

Analytica Chimica Acta 397 (1999) 61–72

ANALYTICA CHIMICA ACTA

www.elsevier.com/locate/aca

Excitation-emission matrix fluorescence based determination of carbamate pesticides and polycyclic aromatic hydrocarbons

Renee D. JiJi, Gary A. Cooper, Karl S. Booksh *

Department of Chemistry and Biochemistry, Arizona State University, Tempe, AZ 85287-1604, USA

Received 1 September 1998; received in revised form 25 January 1999; accepted 1 February 1999

Abstract

The ability to accurately quantitate trace pesticides and polycyclic aromatic hydrocarbons (PAHs) by excitation–emission matrix (EEM) fluorescence spectroscopy, when coupled with parallel factor analysis (PARAFAC) deconvolution of the EEM spectra, is demonstrated and discussed. Two EEM fluorometers were investigated. One fluorometer, using a cuvette cell sample holder, realized limits of detection of 1.1, 6.6, and 13 ppb for 1-naphthol, carbaryl, and carbofuran in methanol mixtures, respectively. 0.2 ppb limits of detection were also observed for three PAHs. With this fluorometer, the PARAFAC model was employed to resolve the analyte spectra from overlapping fluorescence signals and Raman scattering profiles. Employing a second fluorometer with a fiber-optic probe for remote sampling yielded 10–30 ppb limits of detection for 9 PAHs. The PARAFAC model was required here to resolve the PAH spectra from the instrumental background.

Keywords: Fluorescence; Pesticides; Polycyclic aromatic hydrocarbons; PARAFAC; 3-Way Calibration

1. Introduction

Fluorescence spectroscopy is a promising technique for environmental analyses. Among the benefits of fluorescence spectroscopy is the adaptability to field measurements, the high sensitivity to a wide array of potential analytes, and, in general, the avoidance of consumable reagents and extensive sample pretreatment. While no battery operated, hand held, excitation–emission matrix (EEM) fluorometer is currently on the market, portable fluorometers can be constructed without moving parts to avoid misalignment problems and with fiber-optic probes that permit remote observations [1–3]. Examples of potential analytes accessible by fluorescence spectroscopy include dissolved organic material (DOM), [4,5] polycyclic aromatic hydrocarbons (PAHs), [1,2,6–8] and pesticides [9,10]. DOM and PAHs, in particular, are naturally fluorescent in aqueous solutions and their high molecular quantum yield permits detection of trace quantities without sample pretreatment or concentration [11].

Fluorescence spectroscopy compares favorably to other techniques in analyses for PAHs and certain pesticides. EPA approved methods for PAH quantitation entail liquid-liquid or solid phase extraction for preconcentration prior to chromatographic analysis [12]. Methods exist for both gas chromatography (EPA method 8100) and liquid chromatography (EPA method 8310) where 10 parts-per-trillion

* Corresponding author. Tel.: +1-480-965-3058; fax: +1-480-965-2747
E-mail address: booksh@asu.edu (K.S. Booksh)

0003-2670/99/$ – see front matter
PII: S0003-2670(99)00392-X

detection limits can be achieved [12]. Comparatively, PAH detection limits for laser induced fluorescence, laser induced fluorescence with a fiber optic probe, and Xe lamp induced fluorescence have been observed in aqueous solutions at 10 ppt, [1] 10 ppb, [13] and 10 ppb, [8], respectively, without preconcentration. By relying on analyte extractions from the aqueous phase, neither chromatographic method is capable of real time, in situ analysis; fiber-optic fluorescence probes are currently employed for real-time in vivo analyses to detect oil and fuel spills [1,14]. Furthermore, both the chromatographic methods consume carrier solvents for analytic separation and sample extraction.

Quantitation of pesticides in environmental samples is a more difficult task than quantitation of PAHs. EPA methods with sub ppt detection limits exist that employ gas chromatography (EPA method 515.1) and liquid chromatography (EPA methods 531.1, 632, and 8318). Like chromatographic analysis of PAHs, extraction is essential [15]. However, GC based analysis of many carbamates is hindered by the thermal degradation of the analytes and precolumn derivation is required [15,16]. Fluorescence spectroscopy is an intriguing alternative to chromatographic quantitation of aromatic pesticides. Many pesticides are either naturally fluorescent [9] or photodegrade into fluorescent byproducts [10,17]. Postcolumn reaction or UV photolysis induced fluorescence is often employed in liquid chromatographic analysis to increase the sensitivity of the method [18,19]. The same postcolumn fluorophore inducing reactions employed in liquid chromatography can be employed to generate analytically useful fluorophores in sample extracts for fluorescence analyses.

However, the wide application of fluorescence techniques for environmental monitoring has been limited by the lack of selectivity of fluorescence spectroscopy. The broad character of both the excitation and emission fluorescence bands curtails the possibility of finding a unique excitation and emission wavelength combination for each potential analyte. This is particularly true due to the ubiquitous, highly fluorescent DOM in natural waters. To over come the problems associated with the broad fluorescent spectra, two solutions have been proposed. The first solution is instrumental in nature. Selectivity is enhanced by employing synchronous scanning fluorescence spectroscopy instead of excitation or emission fluorescence spectroscopies [2,7,9]. Here the differential energy in scanning is chosen to optimize resolution among the species present. Accurate calibration and prediction may then be facilitated by incorporating multivariate calibration methods such as principal component regression or partial least squares regression [6,20]. The second solution combines collection of an entire excitation–emission matrix (EEM) fluorescence spectrum with advanced multi-way spectral deconvolution and calibration algorithms. This is the approach addressed in this paper.

In the following text, the determination of target carbamate pesticides (carbaryl, carbofuran, and the degradation product 1-naphthol) and PAHs (anthracene, pyrene, fluoranthene, and chrysene) via EEM fluorescence spectroscopy with 3-way spectral deconvolution and calibration is discussed'. The limits of detection and ability of parallel factor analysis (PARAFAC) [21,22]. to resolve highly overlapped spectral profiles are demonstrated. Of particular interest is the capability of PARAFAC applied to EEM fluorescence data to provide accurate analytic estimations in the presence of overlapping, uncalibrated spectral interferences.

2. Theory

2.1. Single measurement EEM fluorescence

Single measurement EEM fluorometry was introduced by Christian et al. in the 1970s [23]. A broadband light source, such as a Hg(Xe) or Xe lamp, is focused on a the excitation spectrometer. The exit slit of the spectrometer is rotated 90° to spatially disperse the light, once focused, across the sample. The emitted fluoresce is collected perpendicular to the excitation light and focused into a second spectrometer. The entire EEM spectrum can, hence, be recorded by a two dimensional type of detector. Analytical utility was initially limited, however, by the absence of imaging spectrographs and 2-dimensional array semiconductor detectors [24].

There are three key performance differences between single measurement EEM fluorometers and scanning fluorometers that can collect entire EEM spectra. First, single measurement EEM fluorometers require imaging optics. Without imaging optics significant spectral distortion will occur everywhere but

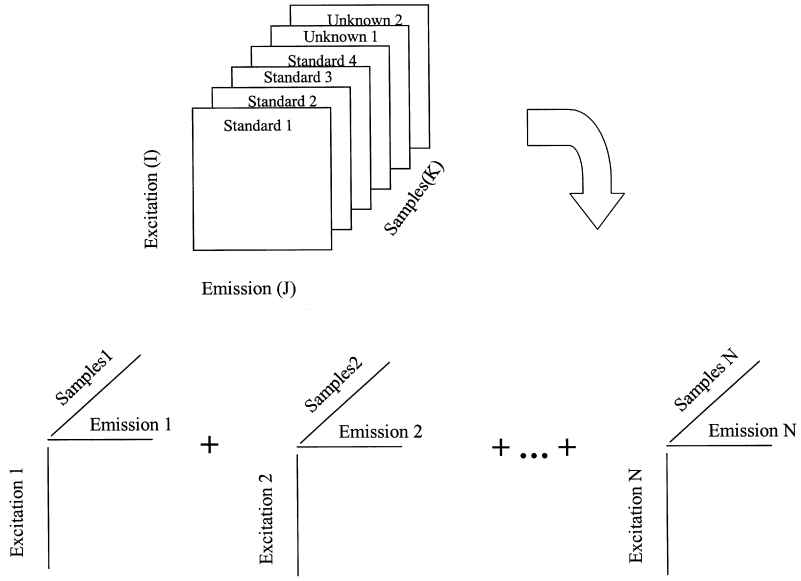

Fig. 1. Pictorial representation of the decomposition of a data matrix into *N* sets of triads.

the center of the recorder EEM image. Second, single measurement EEM fluorometers are significantly quicker in recording an EEM spectrum. Third, single measurement EEM fluorometers lack the baffles and filters to reduce the stray and scattered light. Consequently, recorded EEM spectra have relatively intense Rayleigh and Raman lines compared to scanned EEM spectra.

2.2. 3-Way deconvolution and calibration

The benefits associated with 3-way spectral deconvolution and calibration are well documented and critiqued [25–27]. Primary among these benefits is the 'second order advantage.' In short, the second order advantage allows accurate estimation of analyte concentration in the presence of unknown, uncalibrated spectral interferents. This advantage is derived from the mathematical uniqueness of the 3-way PARAFAC model solution [28] and has been demonstrated on EEM fluorescence data [8,29].

The PARAFAC model is applied to a 3-way data cube, $\mathbb{R}$. In the case of EEM fluorescence, $\mathbb{R}$ is dimensioned *I* excitation wavelength by *J* emission wavelength by *K* samples. An appropriate data set consists of a number of spectra that may be from either mixtures or pure compounds and any spectra from unknown samples that may contain a few unknown, uncalibrated interferents. This is shown pictorially in Fig. 1. The PARAFAC model decomposes $\mathbb{R}$ into *N* sets of triads:

$$R_{ijk} = \sum_{n=1}^{N} X_{in} Y_{jn} Z_{kn} + E_{ijk} \tag{1}$$

Here *N* is a user adjustable parameter that equals the number of 'factors' in the model. A 'factor' can be the fluorescence of an analyte, the fluorescence of an interferent, or part of the instrumental background (i.e. the Raman scattering or stray light). Each of the *N* columns of **X** correspond to excitation profiles of the *N* factors in the sample set. Each of the *N* columns of **Y** correspond to the emission profiles of the *N* factors in the sample set. The matrix $\boldsymbol{x}_n \boldsymbol{y}_n^T$ is the normalized (unit area) estimated EEM spectrum of the *n*th factor. The *n*th column of **Z** corresponds to the contribution of the *n*th factor in each of the *K* samples. Thus, by simultaneously decomposing the standard and unknown spectra, the EEM fluorescence signal from the unknown sample can be uniquely resolved from that of any overlapping, uncalibrated interferents. For calibration and estimation, the subset of the *K* entries in the appropriate column of **Z** that correspond to the analyte are regressed against the known analyte concen-

tration. Either a linear or a nonlinear univariate regression model may be employed [30]. Unknown sample estimation is performed by interpolation of the subset of the *K* entries from the same column of **Z** that correspond to the unknown samples. The resolved excitation and emission profiles can be employed for verification of the association of each of the *N* columns in **Z** with particular species profiles. A more detailed explaination of the PARAFAC modeling procedure can be found in a tutorial by Bro [25].

The least-squares estimates of the parameters in Eq. (1) can be determined by the iterative PARAFAC algorithm. With this algorithm, the number of factors, *N*, is predetermined by the analyst. In the first step of the algorithm, initial estimates of **X** and **Y** are assumed. These estimates may be provided by a random number generator or derived through the direct trilinear decomposition [31]. In the main iterative loop, the current estimates of **X** and **Y** are employed to calculate the least squares estimate of **Z**. Subsequently, a new least-squares estimate of **X** is calculated from the current estimates of **Y** and **Z**. Then, the new least squares estimate of **Y** is determined from the current estimates of **X** and **Z**. Constraints, such as non-negativity of spectral or concentration estimates, may be applied at any step of the iterative loop.

The main loop is repeated until the convergence criteria are met. One popular criterion for convergence is based in the unconstrained correlation coefficient.[32] This method is numerically stable and is more rapidly calculated than criteria based on model fit. Here the correlation coefficients between the estimated **X**, **Y**, and **Z** matrices from successive iterations is calculated. Convergence is assumed when the product of the three correlation coefficients is greater than $1-\epsilon$, where ϵ is set arbitrarily small (1×10^{-9} in this application). Usually this occurs within 1000–2000 iterations.

3. Experimental

3.1. EEM fluorometers

The first EEM fluorometer was constructed in the manner of Murowski, et al [24]. Light from a 75 W Xe arc lamp (Acton Research, Acton, MA.) was collected through the 2.75 mm entrance slit of a 150 mm imaging spectrograph (Acton Research, Acton, MA.). This excitation spectrograph was fitted with a 600 gr/mm ruled grating blazed at 300 nm. The spectrograph was modified such that the 1mm exit slit is rotated 90°. The excitation spectrograph was attached to a sample chamber (Acton Research, Acton, MA.) where the excitation spectrum was focused onto a cuvette. The emitted fluorescence was collected perpendicular to the excitation spectrum and focused onto the 1mm slit of a second 150 mm imaging spectrograph (Acton Research, Acton, MA.). The emission spectrograph contained a 600 gr/mm ruled grating blazed at 500 nm. The resultant 60×80 nm EEM spectrum was recorded on a thermoelectrically cooled, SBIG ST6 CCD camera (Santa Barbara Instrument Group, Santa Barbara, CA.) The camera was computer controlled through KestrelSpec 3.2 (Catalina Scientific, Tucson, AZ).

The second EEM fluorometer is similar to the one described above except that a fiber-optic sampling probe replaces the cuvette sample holder. A 150 W Xe arc lamp (Oriel , Stratford, CT) served as the excitation source. The 250 mm excitation and emission spectrographs contained 600 gr/mm ruled gratings blazed at 200 and 500 nm, respectively (ISA/Jobin-SPEX, Trenton, NJ). The exit slit of the excitation spectrograph was removed and replaced, perpendicular to the normal slit orientation, with a spaced array of 16 200 μm core low OH fused silica optical fibers (Polymicro Technologies, Phoenix, AZ). The fibers were spaced 250 μm apart such that each excitation fiber carried an 8 nm bandpass of light across a 120 nm window. The distal ends of these fibers were paired with 16 fibers from the distal end of a second identical fiber array that collects the induced fluorescence. Each pair of fibers was secured in a 510 μm inner diameter syringe barrel. These 16 fiber pairs were spaced approximately 1 cm apart to form a 4×4 array at the probe tip. A Parkerized aluminum beam stop was positioned 2.5 cm from the fibers. This served to limit fluorescence cross-talk between the fiber pairs. The emission array is positioned at the slit of the emission spectrograph. The EEM spectrum of each sample is recorded by a 2.5×2.5 cm thermoelectrically cooled CCD detector (ISA/Jobin–SPEX, Trenton, NJ). The detector was binned horizontally such that 16 stripes were recorder, one for each of the fiber pairs.

3.2. Sample preparation and analysis

Technical grade carbaryl (98.4% purity) was obtained from Rhône–Poulenc, 1-napthol (99% purity) and carbofuran (98% purity) were both obtained from Aldrich. Anhydrous reagent grade methanol (Aldrich) was used for all dilutions and all reagents were used without further purification. Stock solutions of carbaryl, 1-napthol, and carbofuran were prepared by diluting 1.4, 1.3, and 1.3 mg respectively in methanol to 100 ml. Seven standard solutions, from 5 to 100 ppb, were prepared for each carbaryl, 1-napthol, and carbofuran. In addition three mixtures containing two of the analytes at 60 ppb each and one mixture containing all three analytes at 60 ppb each, were also prepared. Four replicate EEM spectra were collected for each of the standard solutions, for both carbaryl and 1-napthol. Five replicate spectra were collected for each of the carbofuran standard solutions. Four EEM spectra were collected for each of the four mixtures, and twelve spectra were collected for pure methanol, to be used as blanks. The excitation and emission spectrographs were centered at 270 and 300 nm, respectively, with a 60 s integration time was chosen for the detector.

For the cuvette fluorometer experiment, three PAHs were dissolved in distilled water: anthracene, fluoranthene, and pyrene (Accustandards). Stock solutions were prepared by dissolving 5.0 mg of individual PAHs in methanol. The PAHs were diluted to 20, 50, 100, and 200 ppb concentrations by adding the stock solution by volumetric pipette to a small volume of distilled water in a volumetric flask, filling the flasks to point slightly below the mark with distilled water, then allowing the sample to sit for 30 min before diluting to volume. Two component mixtures consisted of 10 ppb pyrene and varying crysene concentrations.

For the fiber-optic fluorometer experiment, an EPA certified standard kit of 17 PAHs was obtained from Accustandard Corporation. Nine of the compounds were used in the experiment: benzo(k)fluoranthene, anthracene, perylene, fluoranthene, phenanthrene, benzo(a)pyrene, crysene, pyrene, and benzo(g,h,i)perylene. Each was chosen based upon its known region of excitation; all had excitation maxima from 270 to 390 nm. Stock solutions of the 9 PAHs were prepared by dissolving 5.0 mg of the individual compounds in 100 ml of warm (40°C) anhydrous methanol in an 1 l volumetric flask. After dissolution, each solution was allowed to cool to room temperature and then diluted to volume with distilled water.

3.3. Data analysis

Analysis and deconvolution of the EEM spectra were performed in the Matlab 5.1 (MathWorks, Natick, MA) working environment. The PARAFAC decomposition and linear regression programs were written in-house. The programs were executed on IBM compatible computers with Intel Pentium 200 Mhz processors. Prior to importing the data into Matlab, spectra from the cuvette system were converted to ASCII files by internal converters in KestrelSpec; data from the fiber optic system were converted to ASCII files by GRAMS/32 (Galactic Industries, Salem, NH).

4. Results and discussion

4.1. Pesticide analysis; cuvette fluorometer

Recorded EEM spectra of 100 ppb carbaryl, carbofuran, and 1-naphthol in methanol are presented if Fig. 2(a–c), respectively. The intense Rayleigh scattering has been truncated from the upper left corner of the image. Carbaryl, near the center of the images, has an excitation maximum near 270 nm and an emission maximum around 320 nm. The carbaryl spectrum is overlapped by the EEM profile of 1-naphthol, a metabolite of carbaryl. 1-Naphthol has maxima at approximately 280 nm excitation and 340 nm emission and fluoresces with 2.5 times the intensity of the carbaryl. Carbofuran slightly overlapps carbaryl and is highly overlapping with the Raman band around 270 nm excitation and 300 nm emission. Carbofuran exhibits only 40% of the fluorescence of carbofuran. Consequently, traditional fluorescence calibration of mixtures of these three analytes is not trivial. There are no excitation-emission wavelength pairs that are truly unique to each of the compounds.

One option for calibration is to employ PARAFAC deconvolution of the EEM spectra to resolve each of the analyte profiles from any uncalibrated spectroscopic interferents (i.e. Raman scattering, a fluorescent

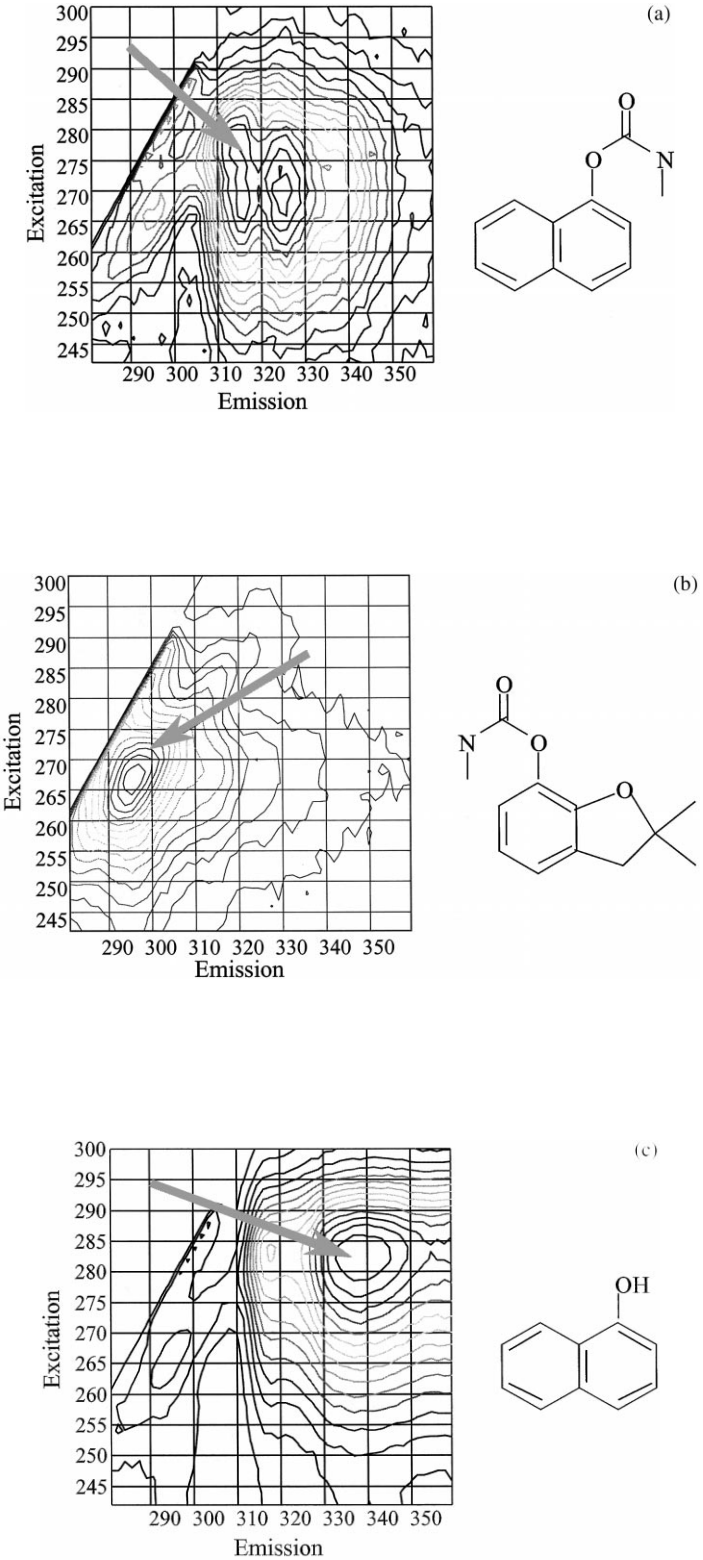

Fig. 2. Recorded EEM spectra of 100 ppb solution of (a) carbaryl, (b) carbofuran, and (c) 1-naphthol in methanol.

Table 1
Figures of merit for neat pesticide calibrations

	LOD[a] (ppb)	RMSE[b]	Sensitivity[c] (total counts/ppb)
Carbaryl	3.8	2.9	3.8×10^4
Carbofuran	10.7	3.8	1.6×10^4
1-Naphthol	1.5	1.9	9.3×10^4

[a] LOD is determined by three standard deviations of the blank (11 d.f.).
[b] RMSE is calculated from errors of fit in the calibration model (38 d.f for carbaryl and 1-naphthol, 45 d.f. for carbaryl).
[c] One count is equal to one part in 2^{16} of the dynamic range for each pixel. Total counts are the integrated area under the resolved EEM profile for the given analyte.

background, or other fluorescent analytes). Ideally, spectral deconvolution methods would be employed that efficiently incorporate the Rayleigh and Raman scattering in the calibration model. It should be noted that the PARAFAC based methods effectively handle spectroscopic interferents that can be directly modeled by Eq. (1). However, Rayleigh and Raman scattering are difficult to model via PARAFAC; there are no intrinsic profiles in either the *X*- or *Y*-order to extract. For this reason, all spectra were pretreated by assigning a single fixed value to the Rayleigh scattering region. The effects of the Raman scattering were minimized, but not eliminated, by subtracting the mean blank from all spectra. Research is currently being performed to determine the best way to apply three-way calibration methods when the Rayleigh and/or Raman scattering cannot be eliminated.

Calibration of carbaryl and 1-naphthol required only a 1 factor PARAFAC model for calibration as these analytes are well resolved from the Raman scattering. Carbofuran completely overlapps the Raman region and a two factor model was found to be optimal. Table 1 lists the limit of detection (LOD), root mean squared errors (RMSE) of calibration, and sensitivity for calibrations of neat carbaryl, carbofuran, and 1-naphthol solutions. Not surprisingly, there is a strong inverse correlation between sensitivity and LOD. All three calibrations appeared very linear over the tested range of 0 to 100 ppb. The one possible exception is 1-naphthol. Fig. 3 shows a plot of intensity of the resolved 1-naphthol spectrum in each sample versus assumed concentration. The 100 ppb standards display a slight negative deviation from linearity. Also shown are the resolved spectral intensities of three outliers in the 1-naphthol standards (clear circles). These three standards are removed from consideration when determining the best calibration curves. No other samples (for any standard or mixture) were flagged as potential outliers or removed from the data set.

Simultaneous deconvolution of the carbaryl and 1-naphthol standards tests the capability of the PARAFAC modeling method to avoid false positives in low concentration applications. The 12 blanks, 28 carbaryl standards, and 28 1-naphthol standards were combined in one data set and decomposed with a two factor PARAFAC model. For a calibration curve constructed from the blanks and 1-naphthol standards, a LOD of 0.9 ppb and a RMSE of 1.8 ppb were observed. This is comparable to the LOD and RMSE observed from calibration following deconvolution of only the 1-naphthol standards. In this exercise, the carbaryl standards were treated as unknown samples. It is expected that the predicted 1-naphthol concentration in these samples would not be statistically greater than the LOD. In fact, only the samples containing 100 ppb carbaryl contained statistically significant 1-naphthol estimates (3 ppb). Concurrently, the data can be reinterpreted by treating carbaryl as the analyte and the 1-naphthol standards as the unknowns. The LOD and RMSE for carbaryl are 2.4 and 2.0 ppb, respectively; comparable to the figures of merit for the 1 factor (standards only) calibration curve. However, estimation of carbaryl in the

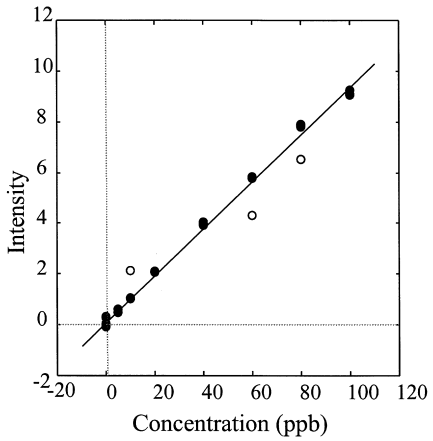

Fig. 3. Calibration curve for 1-naphthol. Outlier standards are indicated by open circles. Intensity is given in arbitrary units related to the total intensity of the resolved analyte spectrum.

Table 2
(a) Figures of merit for simultaneous analysis of all blanks, standards and mixtures with a 4 factor PARAFAC and (b) non-negative least squares PARAFAC model

Analyte	Sensitivity[a] total counts/ ppb	LOD[b]	RMSE: carbaryl standards (ppb)	RMSE: carbofuranstandards (ppb)	RMSE:1-naphthol standards (ppb)	% RMSE: mixtures
(a)						
Carbaryl	3.8×10^4	6.6	2.7[c]	5.6[d]	9.2[d]	4.9[d]
Carbofuran	1.6×10^4	13	7.0[d]	4.2[c]	6.9[d]	9.2[d]
1-Naphthol	9.2×10^4	1.1	0.91[d]	0.54[d]	1.9[c]	5.4[d]
(b)						
Carbaryl	3.2×10^4	0	2.4[c]	3.3[d]	8.2[d]	3.6[d]
Carbofuran	1.4×10^4	3.4	11[d]	5.2[c]	7.1[d]	8.4[d]
1-Naphthol	8.8×10^4	0	0.81[d]	0.62[d]	1.8[c]	5.6[d]

[a] One count is equal to one part in 2^{16} of the dynamic range for each pixel. Total counts are the integrated area under the resolved EEM profile for the given analyte.
[b] LOD is determined by three standard deviations of the blank (11 d.f.).
[c] Root mean squared error of fit for the calibration curve.
[d] Root mean squared error of estimation.

1-naphthol standards shows a RMSE of 8.4 ppb for all samples with a maximum error of 14 ppb for the 100 ppb 1-naphthol samples. The errors for carbaryl estimation in 1-naphthol samples are greater than the errors for estimating 1-naphthol in carbaryl samples because the 1-naphthol signal is 2.5 times as intense as the carbaryl fluorescence and 1-naphthol has a greater overlap of the carbaryl than does carbaryl overlap 1-naphthol.

Table 2(a) presents the figures of merit from the simultaneous decomposition of all 119 EEM spectra with a 4 by factor PARAFAC model. Applying the more complicated 4 factor PARAFAC model does not degrade the sensitivity or the RMSE of fit for the construction of the calibration curve. Compared to application of the PARAFAC model to neat standards, there is actually a slight decrease in the LOD (Table 1, column 2 versus Table 2, column 3). Investigation of the RMSE of prediction for estimation of analyte concentration in the other standards shows that 1-naphthol may significantly bias estimation of carbaryl near the LOD. However, the RMSE of prediction for all other analyte-interferent combinations is less than the LOD for the designated analyte. The worst case scenario is the interference of carbaryl for the prediction of 1-naphthol. Here the RMSE of 1-naphthol prediction, in dilute carbaryl samples spanning the range of 5–100 ppb carbaryl, 83% of 1-naphthol's LOD. Similarly, prediction of pesticide and metabolite ratios in methanol solutions containing 60 ppb either two or three of the analytes under investigation show RMSE of prediction between 5 and 10%.

That the four factor PARAFAC model is appropriate for the data set is supported by observing the resolved excitation and emission spectra presented in Fig. 4(a,b). The resolved spectral profiles all look reasonable and qualitatively agree with the observed excitation spectra (rows) and emission spectra (columns) in Fig. 1.

Further evidence of the model quality and stability is observed by comparing quantitative and qualitative results of the unconstrained PARAFAC model (above) to the model results after constraining the PARAFAC model to return only non-negative estimates of the excitation spectra, emission spectra, and analyte concentrations. These non-negative least squares results are shown in Table 2(b). The sensitivity, RMSE of prediction and RMSE of calibration are all very similar to the results from the unconstrained model. Also, the derived spectral profiles are also very similar to the spectral estimates from the unconstrained application of the PARAFAC model. Only the LOD differ between the two applications. With the non-negativity constraints, the PARAFAC model always estimated the 1-naphthol and carbaryl concentration in the blanks to be identically 0 ppb.

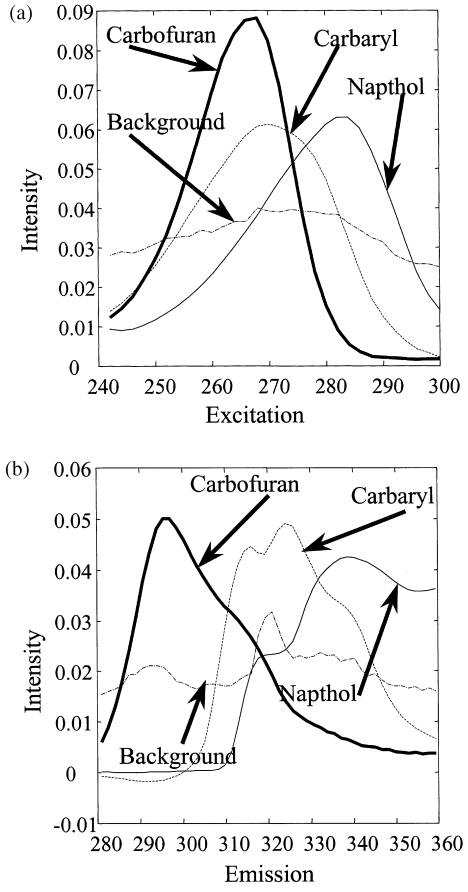

Fig. 4. Resolved (a) excitation and (b) emission spectra from mixtures of (bold) carbofuran, (natural) 1-naphthol, (dashed) carbaryl, and (dash-dot) instrumental background.

4.2. PAH analysis; cuvette fluorometer

The figures of merit for calibration of three sets of aqueous PAH solutions are presented in Table 3. The PAHs studied exhibit a strong red-shift in the fluorescence spectra. Therefore, with no overlap between the fluorescence profiles and the Rayleigh and Raman scattering, a one factor PARAFAC model is sufficient for calibration of the neat standards. From this calibration curve, a 0.2 ppb LOD in water, calculated based on 3σ of the blanks, was observed for all three analytes. The LOD for the aqueous PAHs is less than the LOD of the pesticides in methanol since the PAHs are much more fluorescent – the sensitivity of the PAHs is an order of magnitude greater than the sensitivity of the pesticides. Note that the PAH LOD could be even lower if solid phase extraction and redisolution into another solvent were performed. While these steps would greatly improve the LOD by preconcentrating the analyte and enhancing the quantum yield, extraction is reagent and labor intensive compared to direct analysis.

As with the pesticide samples, accurate analyte prediction in the presence of uncalibrated, highly overlapping spectra can performed. Fig. 5(a) presents the calibration curve derived from the 2 factor PARAFAC decomposition of 4 pyrene standards, 2 blanks, and 2 pyrene/crysene mixtures. Each of the mixtures contained the same pyrene concentration and a different crysene concentration. The mixture samples were treated as the unknown and not used to construct the calibration model. The overall error in estimating the pyrene concentration in the mixtures is 1.03 and 0.99 ppb. The difference between the two estimated concentrations (0.04 ppb) is less than the standard deviation of estimation in the model (0.220 ppb). Concurrently, the difference between the estimated pyrene concentrations is less than the errors observed between duplicate measurements. This can be seen by comparing the spread in the 24.5 ppb samples to the spread of the two mixtures. Therefore, it can be seen that the overlapping crysene interferents has a negligible effect on the accuracy of estimation when PARAFAC is employed to resolve the spectra prior to calibration. For the sake of comparison, the resolved emission spectra are shown in Fig. 5(b). The estimated spectral profiles agree with the crysene and pyrene emission spectra collected from neat samples.

4.3. PAH analysis; fiber-optic probe

Preliminary figures of merit for 9 PAHs analyzed with the fiber-optic probe incorporated in a EEM fluorometer are presented in Table 4. The LOD for the fiber optic fluorometer is probably on order of magnitude greater than can ultimately be achieved. There were not sufficient blanks collected to determine a reliable LOD based on the standard deviation of the blank. Consequently, a pessimistic LOD based on the standard deviation of prediction was substituted. Also, there are improvements that can be incorporated into the fiber-optic probe itself. The excitation fibers can be replaced with solarization resistant optical fibers

Table 3
Figures of merit for neat PAH calibrations from spectra collected with the cuvette based fluorometer

Analyte	Sensitivity[a] total counts/ ppb	LOD[b] (ppb)	RMSE[c] (ppb)
Anthracene	6.2×10^4	0.2	0.06
Fluoranthene	1.8×10^4	0.2	0.08
Pyrene	5.1×10^5	0.2	0.06

[a] One count is equal to one part in 2^{16} of the dynamic range for each pixel. Total counts are the integrated area under the resolved EEM profile for the given analyte.
[b] LOD is determined by three standard deviations of the blank (8 d.f.).
[c] Root mean squared error of fit for the calibration curve.

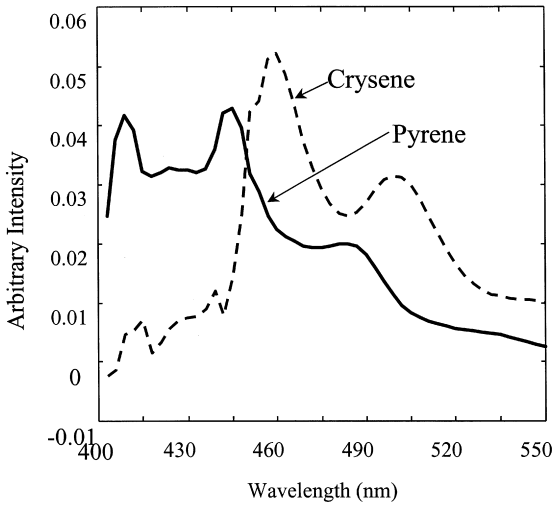

Fig. 5. Resolved emission spectra of (bold) pyrene and (dashed) crysene from mixtures of the two PAHs.

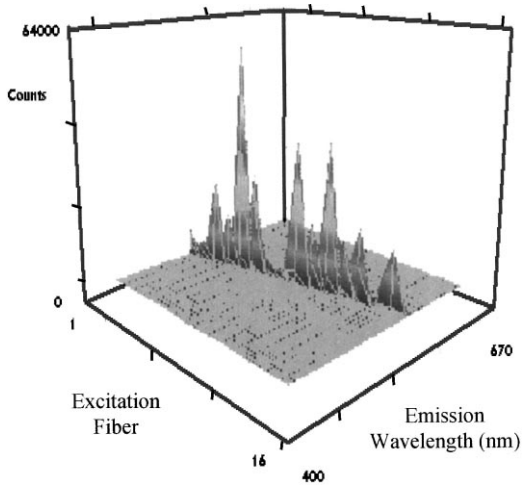

Fig. 6. Raw CCD image of Rayleigh scattering. Each peak corresponds to the light returning from one fiber pair.

that transmit better in the UV. The fibers employed here were optimal for visible/IR light. Improvements can be further gained by better polishing and aligning of the fiber pairs. These fibers were polished by hand and little effort was spent aligning the fibers in the syringe barrels. This resulted in a drastic difference in photo-return among the fiber pairs. The raw CCD image of returning Rayleigh scattering from a starch solution is shown in Fig. 6.

PARAFAC analysis of the data collected with the fiber-optic fluorometer requires an addition one or two factors to account for the stray light background that enters the system. The stray light background is inevitable unless the probe is operated in complete darkness. It should be noted that this background comes primarily from the ambient room light, not from cross-talk between the fibers. Regardless, the PARAFAC model can easily account for this spectral background any still yield unbiased concentration estimates for unknown samples.

5. Conclusions

While the feasibility of employing PARAFAC modeling techniques with EEM fluorescence to accurately deconvolve and quantitate spectrally overlapping fluorophores has been discussed in nearly ideal cases, there are still important issues that are being addressed. The PARAFAC model assumes no interactions between fluorescence species. However, intermolecular interactions do occur as dimerization, energy transfer, and absorbance of emitted fluorescence. More complex generalizations of the PARAFAC model are be-

Table 4
Figures of merit for neat PAH calibrations from spectra collected with the optical fiber based fluorometer

Analyte	Sensitivity[a] total counts/ ppb	LOD[b] (ppb)	RMSE[c] (ppb)
Benzo(a)pyrene	1.1×10^4	13	7
Benzo(b)fluoranthene	8.8×10^4	8	1
Benzo(k)fluoranthene	1.3×10^4	32	17
Benzo(g,h,i)perylene	2.6×10^4	8	3
Crysene	6.5×10^4	21	9
Dibenzene(a,h)anthracene	4.6×10^3	18	15
Fluoranthene	3.0×10^4	14	7
Phenanthrene	3.4×10^3	37	20
Pyrene	7.1×10^4	21	12

[a] One count is equal to one part in 2^{16} of the dynamic range for each pixel. Total counts are the integrated area under the resolved EEM profile for the given analyte.
[b] LOD is determined by propagation of errors (from the fit of the calibration curve) as three standard deviations of prediction for a hypothetical blank sample.
[c] Root mean squared error of fit for the calibration curve.

ing investigated that model these phenomena. Another unresolved issue in the application of multi-way modeling techniques is the determination of optimal model complexity. For example, what is the best way to incorporate any overlapping Raman signal into the modeling process and how to best model systems, such as fluorescence quenching in metal–humic material complexes, where one molecule can have multiple fluorescence centers? As these issues, and other issues raised by Smilde, [27] are resolved, multi-way sensors and multi-way calibration should become increasingly prevalent in every analytical chemist's toolbox.

Acknowledgements

The authors gratefully thank the Camile and Henry Dreyfus Foundation for financial support. The authors also thank Rhône-Poulenc for donation of the bulk carbaryl.

References

[1] T.A. Taylor, G.B. Jarvis, H. Xu, A.C. Bevilacqua, J.E. Kenny, Laser-based fluorescence EEM instrument for in-situ groundwater monitoring, Analytical Instrumentation 21 (1993) 141–162.
[2] A.D. Campiglia, T. Vo-Dihn, Fiber optic sensor for laser-induced room-temperature phosphorescence detection of polycyclic aromatic compounds, Talanta 43 (1996) 1805–1814.
[3] Z.Y. Zhu, M.C. Yappert, Sensitivity enhancement in capillary/fiber-optic fluorometric sensors, Anal. Chem. 66 (1994) 761–764.
[4] J.C.G.E. daSilva, A.A.S.C. Machado, C.J.S. Oliveria, Study of the interaction of a Soil Fulvic Acid with UO22+ by Self Modeling Mixture Analysis of Synchronous Molecular Fluorescence Spectra, Analyst 121 (1996) 1373–1379.
[5] S.E. Cabaniss, Synchronous fluorescence spectra of metal-fulvic acid complexes, Environ. Sci. Tech. 26 (1992) 1133–1139.
[6] J. Guiteras, J.L. Beltran, R. Ferrer, Quantitative multicomponent analysis of polycyclic aromatic hydrocarbons in water samples, Anal. Chim. Acta 361 (1998) 233–240.
[7] J.J.S. Rodriguez, J.H. Garcia, M.M.B. Suarez, A.B. Marin-Lazaro, Analysis of mixtures of polycyclic aromatic hydrocarbons in sea-water by synchronous fluorescence spectrometry in organized media, Analyst 188 (1993) 917–921.
[8] K.S. Booksh, A.R. Muroski, M.L. Myrick, Single-measurement EEM spectrofluometer for determination of hydrocarbons in ocean water. 2. calibration, single-measurement EEM spectrofluometer for determination of hydrocarbons in ocean water. 2. calibration and quantitation of naphthalene and styrene, Anal. Chem. 68 (1996) 3539–3544.
[9] L.A. Files, J.D. Winefordner, Feasibility study of constant energy synchronous luminescence spectrometry for pesticide determination: application to carbaryl, naphthol, and carbofuran, J. Agric. Food Chem. 35 (1987) 471–474.
[10] A. Coly, J.J. Aaron, Cyclodextrin-enhanced fluorescence, Cyclodextrin-enhanced fluorescence and photochemically-induced fluorescence determination of five aromatic pesticides in water, Anal. Chim. Acta 360 (1998) 129–141.
[11] T.D. Downare, O.C. Mullins, Visible and near-infrared fluorescence of crude oils, Appl. Spectros. 49 (1995) 754–764.

[12] Test Methods for evaluating Solid Waste. Vol. 1B: Laboratory Manual Physical/Chemical Methods, 3rd ed., US Environmental Protection Agency, 1986.
[13] C.L. Stevenson, T. Vo-Dinh, Analysis of polynuclear aromatic compounds using laser-excitated synchronous fluorescence, Anal. Chim. Acta 303 (1995) 247–253.
[14] A. Henderson-Kinney, J.E. Kenny, Spectroscopy in the field: emerging techniques for on-site environmental measurements, Spectroscopy 10 (1995) 32–38.
[15] I. Liska, J. Slobodnik, Comparison of Gas and Liquid Chromatography for Analyzing Polar Pesticides in Water Samples, J. Chromatgr. A. (1996) 733 235-238.
[16] W.P. Cochrane, Application of Chemical Derivatisation Techniques for Pesticide Analysis, J. Chromat. Sci. 17 (1979) 124–137.
[17] A. Coly, J.J. Aaron, Photo-chemical-spectrfluorimetric method for determination of several aromatic insecticides, Analyst 119 (1994) 1205–1209.
[18] C.J. Miles, H.A. Moye, Postcolumn Photolysis of Pesticides for Fluorometric Determination by High-Performance Liquid Chromatography, Anal. Chem. 60 (1988) 220–226.
[19] C.J. Miles, Determination of national survey of pesticides analytes in ground water by liquid chromatography with postcolumn reaction detection, J. Chromatography 592 (1992) 283–290.
[20] C. Sluszny, V. Bulatov, I. Schechter, Classification and quantification of polycyclic aromatic hydrocarbons on quartz and sand particles by direct fourier transform imaging fluorescence, Anal. Chim. Acta 367 (1998) 1–10.
[21] P.M. Kroonenberg, Three-mode Principal Component Analyses. Theory and Applications, DSWO Press: Leiden (1983)
[22] R.A. Harshman, Foundations of the PARAFAC Procedure, UCLA Working Paper on Phonetics 16 (1970) 1–84.
[23] D.W. Johnson, J.B. Callis, G.D. Christian, Rapid Scanning Fluorescence Spectroscopy, Anal. Chem. 49 (1977) 747A–757A.
[24] A.R. Murowski, K.S. Booksh, M.L. Myrick, Single-Measurement EEM Spectrofluometer for Determination of Hydrocarbons in Ocean Water. 1. Instrumentation and Background Correction, Anal. Chem. 68 (1996) 3534–3538.
[25] R. Bro, PARAFAC. Tutorial and Applications, Chemom. Intel. Lab. Syst. 38 (1997) 149–171.
[26] K. Booksh, B.R. Kowalski, Theory of Analytical Chemistry, Anal. Chem. 66 (1994) 782A–791A.
[27] A.K. Smilde, Three-Way Analyses: Problems and Perspectives, Chemo. Intel. Lab. Sys. 15 (1992) 143–157.
[28] J.B. Kruskal, Rank, Decomposition, and Uniqueness for 3-way and N-way Arrays, in: R. Coppi and S. Bolasso (Eds.), Multiway Data Analysis, Elsivier, Amsterdam 1989.
[29] T. Roch, Evaluation of Total Luminescence Data with Chemometrical Methods: a Tool for Environmental Monitoring, Anal. Chim. Acta 356 (1997) 61–74.
[30] K.S. Booksh, Z. Lin, Z. Wang, B.R. Kowalski, Extension of Trilinear Decomposition Method with an Application ti the Flow Probe Sensor, Anal. Chem. (1994) 2561–2569.
[31] E. Sanchez, B.R. Kowalski, Tensorial Resolution: A Direct Trilinear Decomposition, J. Chemom. 4 (1990) 29–45.
[32] B.C. Mitchell, D.S. Burdick, Slowly Converging PARAFAC Sequences: Swamps, Slowly Converging PARAFAC Sequences: Swamps and Two-Factor Degeneracies, J. Chemom. 6 (1992) 155.